Mon. Not. R. Astron. Soc. **359,** 765–780 (2005) doi:10.1111/j.1365-2966.2005.08957.x

An atlas of calcium triplet spectra of active galaxies

A. Garcia-Rissmann,[1⋆] L. R. Vega,[1,2⋆] N. V. Asari,[1⋆] R. Cid Fernandes,[1⋆] H. Schmitt,[3,4⋆] R. M. González Delgado[5⋆] and T. Storchi-Bergmann[6⋆]

[1]*Depto. de Física – CFM – Universidade Federal de Santa Catarina, C.P. 476, 88040-900, Florianópolis, SC, Brazil*
[2]*Observatorio Astronómico de Córdoba, Laprida 854, 5000, Córdoba, Argentina*
[3]*Remote Sensing Division, Code 7210, Naval Research Laboratory, 4555 Overlook Avenue, SW, Washington, DC 20375, USA*
[4]*Interferometric Inc., 14 120 Parke Long Court, 103, Chantilly, VA 20151, USA*
[5]*Instituto de Astrofísica de Andalucía (CSIC), PO Box 3004, 18080 Granada, Spain*
[6]*Instituto de Física, Universidade Federal do Rio Grande do Sul, C.P. 15001, 91501-970, Porto Alegre, RS, Brazil*

Accepted 2005 February 21. Received 2005 February 21; in original form 2004 December 24

ABSTRACT

We present a spectroscopic atlas of active galactic nuclei covering the region around the λλ8498, 8542, 8662 calcium triplet (CaT). The sample comprises 78 objects, divided into 43 Seyfert 2s, 26 Seyfert 1s, three starburst and six normal galaxies. The spectra pertain to the inner ∼300 pc in radius, and thus sample the central kinematics and stellar populations of active galaxies. The data are used to measure stellar velocity dispersions ($\sigma_\star$) with both cross-correlation and direct fitting methods. These measurements are found to be in good agreement with each other and with those in previous studies for objects in common. The CaT equivalent width is also measured. We find average values and sample dispersions of $W_{\rm CaT}$ of 4.6 ± 2.0, 7.0 ± 1.0 and 7.7 ± 1.0 Å for Seyfert 1s, Seyfert 2s and normal galaxies, respectively. We further present an atlas of [S III]λ9069 emission-line profiles for a subset of 40 galaxies. These data are analysed in a companion paper which addresses the connection between stellar and narrow-line region kinematics, the behaviour of the CaT equivalent width as a function of $\sigma_\star$, activity type and stellar population properties.

Key words: galaxies: active – galaxies: kinematics and dynamics – galaxies: Seyfert – galaxies: statistics – galaxies: stellar content.

1 INTRODUCTION

15 years ago, Terlevich, Díaz & Terlevich (1990, hereafter TDT) carried out the first systematic study of the λλ8498, 8542, 8662 absorption lines of the Ca II ion in active galactic nuclei (AGNs). The main focus of that pioneer work on the 'calcium triplet' (CaT) was on the equivalent width of this feature ($W_{\rm CaT}$), which provides both a stellar population diagnostic and a tool to investigate the presence of an underlying non-stellar continuum. Most of the AGNs in the TDT sample were type 2 Seyferts. Their main finding was that $W_{\rm CaT}$ is remarkably similar for Seyfert 2s and normal galaxies, implying that the non-stellar featureless continuum (FC) invoked to account for the dilution of optical absorption lines in these objects either is not featureless at all or somehow disappears between optical and near-infrared (NIR) wavelengths. The interpretation advanced by TDT was that both the optical FC and the CaT lines are produced by a nuclear starburst. Subsequent work by the same group suggests that this may also apply to at least some type 1 Seyferts (Jiménez-Benito et al. 2000), although in the more active of these objects the AGN continuum does cause some dilution of the CaT.

Since then, the existence of starbursts around Seyfert 2 nuclei has been established by both indirect means (Cid Fernandes & Terlevich 1995; Heckman et al. 1995; Oliva et al. 1999) and direct detections of young stars by optical–ultraviolet imaging and spectroscopy (Heckman et al. 1997; González Delgado, Heckman & Leitherer 2001). While these studies confirmed that the optical FC of Seyfert 2s is predominantly due to recent star formation, there are still doubts as to whether the CaT is produced by these starbursts or by older stars in the host galaxy bulge. In other words, it is not clear whether the CaT can be used to diagnose the presence of starbursts. Indeed, the mere fact that $W_{\rm CaT}$ shows little variation among galaxies of widely different morphological and spectroscopic properties indicates that this feature may not be as simple a tracer of stellar populations as initially thought. Recent empirical and theoretical work reinforce this idea (Saglia et al. 2002; Cenarro et al. 2003, 2004; Falcón-Barroso et al. 2003; Michielsen et al. 2003; Thomas, Maraston & Bender 2003; Vazdekis et al. 2003), and show that there is still much to be learned about the CaT behaviour even in normal galaxies.

⋆E-mail: aurea@astro.ufsc.br (AG-R); luis@astro.ufsc.br (LRV); natalia@astro.ufsc.br (NVA); cid@astro.ufsc.br (RCF); hschmitt@css.nrl.navy.mil (HS); rosa@iaa.es (RMGD); thaisa@if.ufrgs.br (TS-B)

A more widespread use of the CaT nowadays is to measure stellar velocity dispersions ($\sigma_\star$). This was the approach followed by Nelson & Whittle (1995, 1996, hereafter collectively referred to as NW) in their comprehensive study of stellar and gaseous kinematics of AGNs. The discovery of the relation between black hole mass ($M_{\rm BH}$) and $\sigma_\star$ (Ferrarese & Merritt 2000; Gebhardt et al. 2000; Tremaine et al. 2002) brought renewed interest in this type of work. Indeed, most of the current observational CaT studies in AGNs are geared towards using this spectroscopic feature as an indirect black hole weighing scale (Ferrarese et al. 2001; Barth, Ho & Sargent 2002, 2003; Filippenko & Ho 2003; Barth et al. 2004; Botte et al. 2004; Nelson et al. 2004; Onken et al. 2004; Barth, Greene & Ho 2005). Finally, velocity dispersions are also useful to investigate stellar populations. Combined with size and luminosity measurements, $\sigma_\star$ allows the estimation of the mass-to-light ratio, which is a strong function of the age in stellar systems. There have been few applications of this idea to AGNs, but the results reported so far seem to fit the scenario where active nuclei tend to be surrounded by stellar populations younger than those typical of elliptical galaxies and bulges (NW; Oliva et al. 1995, 1999).

This brief summary illustrates that there is plenty of motivation to study the CaT in both active and normal galaxies. In this paper we present an atlas of CaT spectra and related data products for a sample of 78 galaxies, most of which have active nuclei. This material is used in a companion paper (Vega et al., in preparation, hereafter Paper II) to address issues such as the connection between nebular and stellar kinematics, the sensitivity of $W_{\rm CaT}$ to stellar population properties, and constraints on the contribution of a non-stellar component to the NIR spectra of AGNs.

This paper is organized as follows. In Section 2 we describe the sample, observations and data reduction. In Section 3 we present our atlas of CaT spectra, as well as [S III]λ9069 emission-line profiles for a subset of the objects. Measurements of stellar velocity dispersions are presented in Section 4, while in Section 5 we present results on the equivalent width of the CaT. Finally, in Section 6 we summarize our main results.

2 OBSERVATIONS

The data presented here were obtained in six runs in three different telescopes: two at the 1.52-m European Southern Observatory (ESO), La Silla (39 galaxies), two at the Kitt Peak National Observatory (KPNO) 2.1-m telescope (25 galaxies), and two at the KPNO 4-m telescope (16 galaxies). Although the original projects had somewhat different specific goals, they all centred on the measurement of the CaT in AGNs. We have thus decided to merge all the CaT-related data in a single atlas containing the nuclear spectra and associated data products, processed in a way as homogeneous as possible. In this section we describe the observations, reduction process and the general sample properties.

2.1 ESO 1.52-m observations

Most of the southern objects in the sample have been observed with the Boller & Chivens spectrograph coupled at the Cassegrain focus ($f/14.9$) of the now extinct 1.52-m telescope, located in ESO, La Silla (Chile), during two runs (2002 March and October). Similar set-ups have been adopted in both runs, with a grating of 900 l mm^{-1} (5) centred at about 7230 Å, giving a dispersion of 1.32 Å pixel^{-1} on the CCD 38 (2688 × 512 pixels^2, each pixel with a 15-μm size). The slit width of 2 arcsec adopted for all the programme objects (which comprise the galaxies and the template stars) provided a resolution $\sigma_{\rm inst}$ of about 56 and 44 km s^{-1} for the spectra of March and October, respectively, as measured through sky emission lines. The slit was always aligned in the east–west direction (position angle = 90°), and was long enough (4.5 arcmin) to guarantee the inclusion of enough sky to allow its subtraction from the galaxy spectra. The plate scale on the CCD was 0.82 arcsec pixel^{-1}, and the wavelengths covered by the observations ranged from ∼6300 to 9500 Å. Wavelength calibration was performed using HeNeArFe lamp spectra taken in each telescope position. A log of the observations is presented in Table 1. A series of velocity standard stars, listed in Table 4, have also been observed with the same set-up and used as templates in the determination of $\sigma_\star$ (Section 4).

Because fringing effects in the NIR can be a serious concern (see below), internal flats made with a quartz lamp have also been acquired (only in the first run) for every telescope pointing. Twilight flats have also been taken, generally at the sunset, to be used for the illumination correction. Spectrophotometric standard stars from Hamuy et al. (1994), Oke (1990), Massey et al. (1988) and Massey & Gronwall (1990) were observed (at least two per night), always with the slit wide open (5–8 arcsec), for flux calibration. Given the variable atmospheric conditions (particularly in the October run) our absolute flux scale is uncertain, but this has no consequence for the results reported in this paper, because we report only relative measurements.

2.2 KPNO 2.1-m observations

A total of 25 northern galaxies were observed on two observing runs with the KPNO 2.1-m telescope, on the nights of 2002 November 12/13–14/15 and 2003 February 17/18–19/20. The observational set-up was the same in both runs, resulting in spectra of similar quality to those obtained for the ESO sample. We used the Gold Camera Spectrograph with grating 35 and a slit width of 2 arcsec. The slit was oriented in the east–west direction during the first run and in the north–south direction in the second run. This configuration gives a plate scale of 0.78 arcsec pixel^{-1}, a spectral resolution of 1.24 Å pixel^{-1} and a wavelength coverage of ∼6800–9300 Å. The spectral resolution for these data is $\sigma_{\rm inst} \sim 57$ km s^{-1}. A log of the observations is presented in Table 2.

The observation of each galaxy was preceded and followed by internal quartz lamp flat-field frames (for fringing corrections) and HeNeAr wavelength calibration frames. In the case of flux and velocity standard stars, which required only short integrations, the fringe pattern does not vary significantly, so we obtained spectra of the quartz and HeNeAr lamps only once, either before or after the observation of the star. During the first observing run (November) we obtained a series of twilight flats, which were used for illumination correction. However, due to bad weather conditions, we were not able to obtain twilight flats during the February run, having to resort to a combination of the programme frames (excluding the regions of the spatial profiles) for the illumination correction.

Throughout the night we observed a series of velocity standard stars of various spectral types (Table 4), using the same slit width used for the observation of the galaxies. Finally, at least three spectrophotometric standard stars were observed every night, using a 5-arcsec slit. We observed BD+17 4708, G191B2B and Feige 34 in the November run and Feige 66, HZ 44, Hiltner 600 and Feige 34 in the February run. As was the case in the ESO observations, not all of the KPNO observations were made under photometric conditions; however, this does not affect the outcome of this project.

Table 1. Log of the ESO 1.52-m telescope observations. Columns 2, 3 and 4 list the activity type, radial velocity (in km s^{-1}) and Hubble class, all extracted from the NED. Column 5 lists the numerical Hubble type, taken from de Vaucouleurs et al. (1991) (except for those marked with asterisks, unavailable in the catalogue, and whose *T* types were attributed by us based on the Hubble morphological type). Column 8 lists a quality flag (see Section 3.1).

Object	Activity	v_{rad} (km s^{-1})	Morph type	*T*	Date	Exp. time (s)	Flag
NGC 526A	Sy1.5	5725	S0 pec?	0.0	2002 Oct 04	(2×)1800	c
NGC 526B	Normal	5669	SB0: pec	0.0	2002 Oct 04	(1×)1500	c
NGC 1125	Sy2	3277	SB(r)0+	−1.0	2002 Sep 30	(3×)1500	c
NGC 1140	H II/Sy2	1501	IBm pec	10.0	2002 Oct 03	(3×)1500	c
NGC 1365	Sy1.8	1636	(R′)SBb(s)b	3.0	2002 Oct 02	(3×)1500	d
NGC 1380	Normal	1877	SA0	0.0	2002 Sep 30	(2×)1500	c
NGC 1433	Sy2	1075	(R′$_1$)SB(rs)ab	2.0	2002 Oct 01	(3×)1500	b
NGC 1672	Sy2	1350	(R′$_1$)SB(r)bc	4.0	2002 Oct 03	(2×)1500	a
NGC 1808	Sy2	1000	(R′$_1$)SAB(s:)b	3.0	2002 Oct 04	(2×)1200	a
NGC 2997	Normal	1087	SA(s)c	5.0	2002 Mar 11	(2×)1200	a
NGC 3081	Sy2	2385	(R′$_1$)SAB(r)0	0.0	2002 Mar 09	(4×)1200	a
NGC 3115	Sy2	720	S0-	−3.0	2002 Mar 11	(1×)600	a
NGC 3256	H II	2738	Pec; merger	?	2002 Mar 12	(1×)900,(1×)1200	b
NGC 3281	Sy2	3200	SAB(rs+)a	1.0	2002 Mar 10	(4×)1200	b
NGC 3783	Sy1	2717	(R′)SB(r)a	1.0	2002 Mar 09	(5×)1200	a
NGC 4507	Sy1.9	3538	SAB(s)ab	2.0	2002 Mar 11	(3×)1800	a
NGC 4593	Sy1	2698	(R)SB(rs)b	3.0	2002 Mar 11	(3×)1800	c
NGC 4748	Sy1 (NLSy1)	4386	Sa	1.0*	2002 Mar 12	(3×)1800	c
NGC 4968	Sy2	2957	(R′)SAB0^0	−2.0	2002 Mar 12	(2×)1800	a
NGC 5135	Sy2	4112	SB(1)ab	2.0	2002 Mar 11	(2×)1800	a
NGC 6300	Sy2	1110	SB(rs)b	3.0	2002 Mar 12	(2×)1800	a
NGC 6814	Sy1.5	1563	SAB(rs)bc	4.0	2002 Oct 04	(3×)1500	b
NGC 6860	Sy1	4462	(R′)SB(r)ab	2.0	2002 Oct 03	(3×)1500	c
NGC 6907	Normal	3161	SB(s)bc	4.0	2002 Set 30	(3×)1500	c
NGG 7130	Sy2/L	4842	Sa pec	1.0	2002 Sep 30	(3×)1500	b
NGC 7172	Sy2	2603	Sa pec sp	1.0	2002 Oct 02	(3×)1500	a
NGC 7184	Normal	2617	SB(r)c	5.0	2002 Oct 02	(3×)1500	a
NGC 7410	Sy2/L	1751	SB(s)a	1.0	2002 Oct 04	(2×)1800	a
NGC 7496	Sy2	1649	(R′:)SB(rs)bc	4.0	2002 Oct 02	(3×)1500	c
NGC 7582	Sy2	1575	(R′$_1$)SB(s)ab	2.0	2002 Oct 03	(2×)1800	a
NGC 7590	Sy2	1596	S(r?)bc	4.0	2002 Sep 30	(3×)1500	a
NGC 7714	H II/L	2798	SB(s)b:pec	3.0	2002 Oct 04	(2×)1200,(1×)1500	b
IC 2560	Sy2	2925	(R′:)SB(r)bc	4.0	2002 Mar 12	(3×)1800	a
IC 3639	Sy2	3275	SB(rs)bc:	4.0	2002 Mar 10	(3×)1800	a
IC 5169	Sy2	3016	(R′$_1$)SAB(r)0+	−1.0	2002 Oct 01	(3×)1500	c
ESO 362G08	Sy2	4785	Sa	1.0*	2002 Mar 09	(4×)1200	a
ESO 362G18	Sy1.5	3790	S0/a	0.0*	2002 Mar 10	(3×)1800	a
MCG-6.30.15	Sy1.2	2323	E-S0	−2.0*	2002 Mar 10	(3×)1800	a
Mrk 1210	Sy2	4046	Sa	1.0*	2002 Mar 11	(3×)1800	b

2.3 KPNO 4-m observations

Finally, we have incorporated into our data set the CaT observations of 14 Seyfert 2s and two normal galaxies taken in the KPNO 4-m Mayall telescope during two runs in 1996. Table 3 describes these observations. The spectra were taken with a dispersion of 1.52 Å pixel^{-1} covering the unvignetted spectral ranges 6600–9100 Å (February 1996 run) and 7400–9800 Å (October 1996 run). The slit width of 1.5 arcsec was set at the parallactic angle. These data were partly described in González Delgado et al. (2001), to which we refer the reader for details of the observations and reduction process.

2.4 Reduction

Two major problems affect observations and data reductions in the NIR region: the significant contamination by atmospheric emission lines and fringing. In this section we describe how we have dealt with these problems in the reduction of the ESO and KPNO 2.1-m data.

Fringing is caused by the back and forth scattering of the NIR light in coated CCDs. Here we adopted a careful procedure to eliminate fringes, or, at least, to minimize their effects. Instead of using dome-flats, we flat-fielded our data using quartz lamp spectra, because fringes (present in all images) tend to change their locations as the telescope moves. Although for every telescope position one lamp flat was taken, in the first ESO run we decided to search for those flats which reduced the fringing patterns in the final spectrum, following the recipe given in Plait & Bohlin (1997) for the Space Telescope Imaging Spectrograph (STIS) observations (where a library of fringing patterns is available for observers). In order to determine the lamp flat that minimized this effect, we performed the reduction and extraction processes using each of them, for every object spectrum; the extracted spectra were then normalized in the region of interest by smoothed versions of themselves (using a 50-pixel boxcar filter), and finally an autocorrelation analysis over the

Table 2. Log of the KPNO 2.1-m telescope observations.

Object	Activity	v_{rad} (km s^{-1})	Morph type	T	Date	Exp. time (s)	Flag
Mrk 40	Sy1	6323	S0 pec	−2.0	2003 Feb 20	(4×)1200	b
Mrk 79	Sy1.2	6652	SBb	3.0	2002 Nov 14	(3×)1200	d
Mrk 372	Sy1.5	9300	S0/a	0.0*	2003 Feb 20	(3×)1200	a
Mrk 461	Sy2	4856	S0	−2.0*	2003 Feb 19	(3×)1200	b
Mrk 516	Sy1.8	8519	Sc	6.0*	2002 Nov 15	(3×)1200	b
Mrk 705	Sy1.2	8739	S0?	−2.0	2002 Nov 15	(3×)1200	c
Mrk 915	Sy1	7228	Sb	3.0*	2002 Nov 15	(3×)1200	b
Mrk 1210	Sy1/Sy2	4046	Sa	1.0*	2002 Nov 13	(3×)1200	a
Mrk 1239	Sy1.5 (NLSy1)	5974	E-S0	−3.0*	2003 Feb 19	(3×)1200	d
UGC 3478	Sy1.2	3828	Sb	3.0	2003 Feb 20	(4×)1200	d
UGC 1395	Sy1.9	5208	SA(rs)b	3.0	2002 Nov 14	(3×)1200	b
UGC 12138	Sy1.8	7487	SBa	1.0	2002 Nov 13	(3×)1200	b
UGC 12348	Sy2	7631	Sa	1.0	2002 Nov 15	(3×)1200	a
NGC 1019	Sy1	7251	SB(rs)bc	4.0	2002 Nov 14	(3×)1200	a
NGC 1142	Sy2	8648	S pec (Ring B)	1.0	2002 Nov 14	(3×)1200	c
NGC 1241	Sy2	4052	SB(rs)b	3.0	2002 Nov 15	(3×)1200	a
NGC 2639	Sy1.9	3336	(R)SA(r)a:?	1.0	2002 Nov 13	(3×)1200	a
NGC 6951	L/Sy2	1424	SAB(rs)bc	4.0	2002 Nov 14	(2×)1200	a
NGC 7469	Sy1.2	4892	(R′)SAB(rs)a	1.0	2002 Nov 13	(3×)1200	a
IRAS 01475-0740	Sy2	5296	E-S0	−3.0*	2002 Nov 13	(3×)1200	c
IRAS 04502-0317	Sy2	4737	SB0/a	0.0	2002 Nov 15	(3×)1200	c
MCG −01-24-012	Sy2	5936	SAB(rs)c:	5.0	2002 Nov 14	(3×)1200	c
MCG −02-08-039	Sy2	8989	SAB(rs)a pec:	1.0	2002 Nov 15	(3×)1200	b
MCG +8-11-11	Sy1.5	6141	SB0	−2.0*	2002 Nov 13	(3×)1200	d
Akn 564	Sy1.8 (NLSy1)	7400	SB	0.0	2002 Nov 14	(3×)1200	d

Table 3. Log of the KPNO 4-m Mayall telescope observations.

Object	Activity	v_{rad} (km s^{-1})	Morph type	T	Date	Exp. time (s)	Flag
Mrk 0001	Sy2	4780	S?	1.0	1996 Oct 11	(2×)1800	a
Mrk 0003	Sy2	4050	S0:	−1.0	1996 Feb 15	(2×)1800	b
Mrk 0078	Sy2	11137	SB	?	1996 Feb 15	(2×)1800	b
Mrk 0273	Sy2/L	11326	Ring Gal pec	?	1996 Feb 15	(3×)1800	c
Mrk 0348	Sy2	4507	SA(s)0/a	1.0	1996 Oct 11	(2×)1800	a
Mrk 0573	Sy2	5174	SAB(rs)0+	−1.0	1996 Oct 11	(2×)1800	a
Mrk 1066	Sy2	3605	SB(s)0+	−1.0	1996 Oct 11	(1×)1800,(1×)900	a
Mrk 1073	Sy2	6998	SB(s)b	3.0	1996 Oct 11	(1×)1800,(1×)900	a
NGC 0205	Normal	−241	dE	−5.0	1996 Feb 15	(1×)300,(2×)600	a
NGC 1068	Sy1/2	1137	SA(rs)b	3.0	1996 Oct 11	(2×)900	a
NGC 1386	Sy2	868	SB(s)0+	−1.0	1996 Oct 11	(2×)1200	a
NGC 2110	Sy2	2335	SAB0-	−3.0	1996 Feb 15	(1×)1800	a
NGC 4339	Sy2	1289	E	−5.0	1996 Feb 15	(1×)300,(2×)600	a
NGC 5929	Sy2	2492	Sab:pec	2.0	1996 Feb 15	(1×)1800,(1×)900	a
NGC 7130	Sy2/L	4842	Sa pec	1.0	1996 Oct 11	(1×)1800	b
NGC 7212	Sy2	7984	S	?	1996 Oct 11	(2×)1800	a

normalized extracted spectrum was made. For spectra where fringing is more conspicuous, the rms in this autocorrelation function reaches higher values. By selecting the spectra whose autocorrelation function had the lowest rms in the CaT region, we automatically selected those with the smallest fringing patterns. This procedure has been shown to slightly improve the final spectra, compared to no fringing correction. In any case, we have verified that these corrections have little effect upon the main data products reported in this paper, i.e. stellar velocity dispersions and the CaT equivalent width.

The subtraction of atmospheric lines can introduce spurious spikes in the extracted spectra, especially near the most intense ones. This is caused by small fluctuations in the width and location of such lines along the spatial axis, so a sky region as close as possible to the extraction window is preferred. Because this often cannot be the case in observations of extended sources, we adopted a careful procedure for background removal. Possible slight misalignments of the dispersion axis along the CCD lines were corrected applying the IRAF task IDENTIFY to all two-dimensional images, and a bidimensional function of order 6 × 6 was fitted using FITCOORDS. Before the fit, we analysed carefully each object's spatial profile, to determine which CCD regions were at (or as close as possible to) the sky level; we only included in the fit the CCD regions of interest (extraction window + background), in order to achieve a better precision (residuals $\leqslant$0.2 Å pixel^{-1}). Finally, we used the task TRANSFORM to apply the wavelength correction to all the images before the

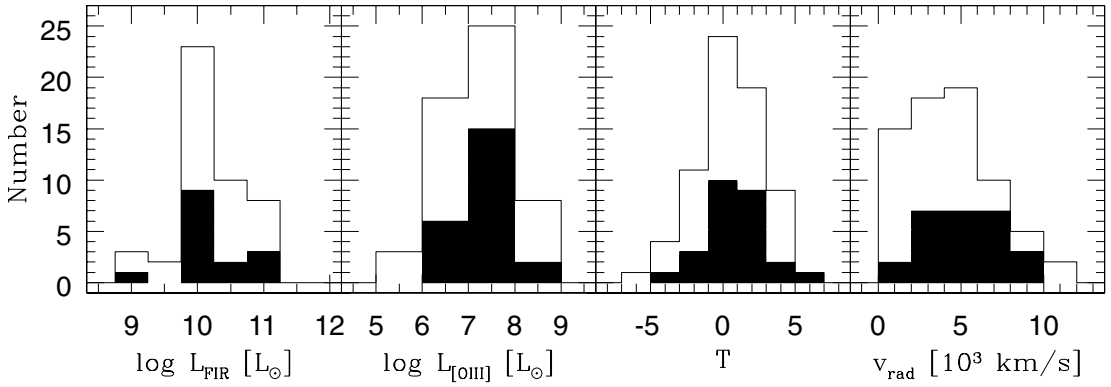

Figure 1. Sample properties. Empty areas correspond to Seyfert 2s and filled boxes to Seyfert 1s.

spectral extraction. Headers from the IHAP/ESO acquisition system have been completed with the task ASTHEDIT from IRAF.

For both the ESO and KPNO 2.1-m data we have extracted nuclear spectra adding the central three pixels (through the optimal extraction algorithm; Horne 1986). This corresponds to spatial scales of 2.46 and 2.34 arcsec for the ESO and KPNO 2.1-m objects, respectively.

The correction for atmospheric extinction was applied using the specific observatory data. Galactic reddening was corrected using the Cardelli, Clayton & Mathis (1989) law with $R_V = 3.1$ and the A_B values from Schlegel, Finkbeiner & Davis (1998) as listed in the NASA/IPAC Extragalactic Database (NED). Atmospheric telluric lines (due mainly to H_2O and O_2) have not been corrected. Nevertheless, as noticed by NW, these affect the measurement of the CaT only in galaxies with redshifts greater than about 8000 km s^{-1}, i.e. in only four out of 78 objects of our sample.

2.5 Sample properties

Tables 1–3 list some properties of the galaxies in the sample, including morphology, recession velocity and activity class, all extracted from the NED, whereas Table 4 shows the velocity standard stars. Because the list of galaxies results from the merging of different observational programmes, none of which aimed at completeness in any sense, the resulting sample is a rather mixed bag of objects. Overall, however, this is a representative sample of Seyfert galaxies in the nearby Universe.

In total, we have 80 spectra of 78 galaxies, divided into 43 Seyfert 2s, 26 Seyfert 1s (including intermediate Seyfert types and narrow-line Seyfert 1s) and nine non-active galaxies, including three starburst nuclei. Mrk 1210 and NGC 7130 were observed twice with different telescopes. Although we keep only the better spectra in the atlas, these duplicate measurements are useful to check uncertainties in our measurements (Section 4.1). Fig. 1 and Table 5 summarize some statistics of the sample, divided into Seyfert 1s, Seyfert 2s and non-active galaxies. The far-IR fluxes were compiled from the NED. [O III]λ5007 fluxes were compiled from a number of papers (Whittle 1992; Storchi-Bergmann, Kinney & Challis 1995; Bassani et al. 1999; Schmitt et al. 2003). In case of duplicate data, we favour measurements obtained under large extractions [to include more of the narrow-line region (NLR) emission] and corrected by reddening. Inevitably, the resulting [O III] luminosities are very inhomogeneous, and should be regarded as uncertain by a factor of ∼2. Table 5 shows that we span a wide range of morphological types, distances, [O III]λ5007 and far-IR luminosities.

Table 4. Velocity standard stars.

Star	Spectral type	Telescope
HD 9737	F0III	KPNO 2.1-m
HD 9748	K0III	KPNO 2.1-m
HD 19136	K0III	KPNO 2.1-m
HD 21910	K0III	KPNO 4-m
HD 23962	K5III	KPNO 2.1-m
HD 31805	F0III	KPNO 2.1-m
HD 39008	K3III	KPNO 2.1-m
HD 39833	G0III	KPNO 2.1-m
HD 41589	K0III	KPNO 2.1-m
HD 62564	K0III	KPNO 2.1-m
HD 71597	K2III	KPNO 4-m
HD 77189	K5III	KPNO 2.1-m
HD 84059	F0III	KPNO 2.1-m
HD 87018	K3III	ESO 1.52-m
HD 89885	K0III	ESO 1.52-m
HD 113678	K0III	ESO 1.52-m
HD 116535	K0III	ESO 1.52-m
HD 116565	K0III	ESO 1.52-m
HD 119171	K0III	KPNO 2.1-m
HD 120572	K3III	ESO 1.52-m
HD 121138	K0III	ESO 1.52-m
HD 121883	K0III	ESO 1.52-m
HD 122665	K5III	ESO 1.52-m
HD 124990	K0III	ESO 1.52-m
HD 127740	F5III	KPNO 2.1-m
HD 128529	K5III	ESO 1.52-m
HD 132151	K0III	ESO 1.52-m
HD 139447	K5III	ESO 1.52-m
HD 143393	K2III	KPNO 4-m
HD 143976	K5III	ESO 1.52-m
HD 151817	K3III	ESO 1.52-m
HD 160413	K3III	ESO 1.52-m
HD 195527	K0III	KPNO 2.1-m
HD 209543	K0III	KPNO 2.1-m
HD 219656	K0III	KPNO 2.1-m
HD 258403	F0III	KPNO 2.1-m

3 THE ATLAS

3.1 CaT spectra

Figs 2–6 present the spectra around the CaT region for all 78 galaxies in our sample. Data from different telescopes are displayed in different plots. As in NW, each panel in these figures includes an example of a velocity standard star observed through the same

Table 5. Statistics of selected properties of the sample, divided into Seyfert 2s, Seyfert 1s and other galaxies. For each property we list the range, mean value and sample dispersion, and the number of objects for which the corresponding quantity was available. Luminosities were computed for $H_0 = 75\,\mathrm{km\,s^{-1}\,Mpc^{-1}}$. All properties were compiled from the NED and the literature.

	Seyfert 2s			Seyfert 1s			Non-AGN		
	N	Range	Mean ± rms	*N*	Range	Mean ± rms	*N*	Range	Mean ± rms
T type	43	(−5,5)	1.0 ± 2.3	26	(−3,6)	1.4 ± 2.1	9	(−5,10)	2.6 ± 4.2
Distance (Mpc)	43	(10,151)	52 ± 36	26	(21,124)	69 ± 29	9	(1,76)	32 ± 21
r_{ap} (pc)	43	(54,715)	285 ± 187	26	(126,734)	414 ± 172	9	(3,459)	193 ± 128
$\log L_{[OIII]}$ ($L_\odot$)	31	(5.6,8.7)	7.2 ± 0.8	23	(6.2,8.1)	7.4 ± 0.6			
$\log L_{FIR}$ ($L_\odot$)	31	(8.9,11.1)	10.2 ± 0.5	15	(9.2,11.2)	10.1 ± 0.5	7	(6.0,11.3)	9.6 ± 1.7

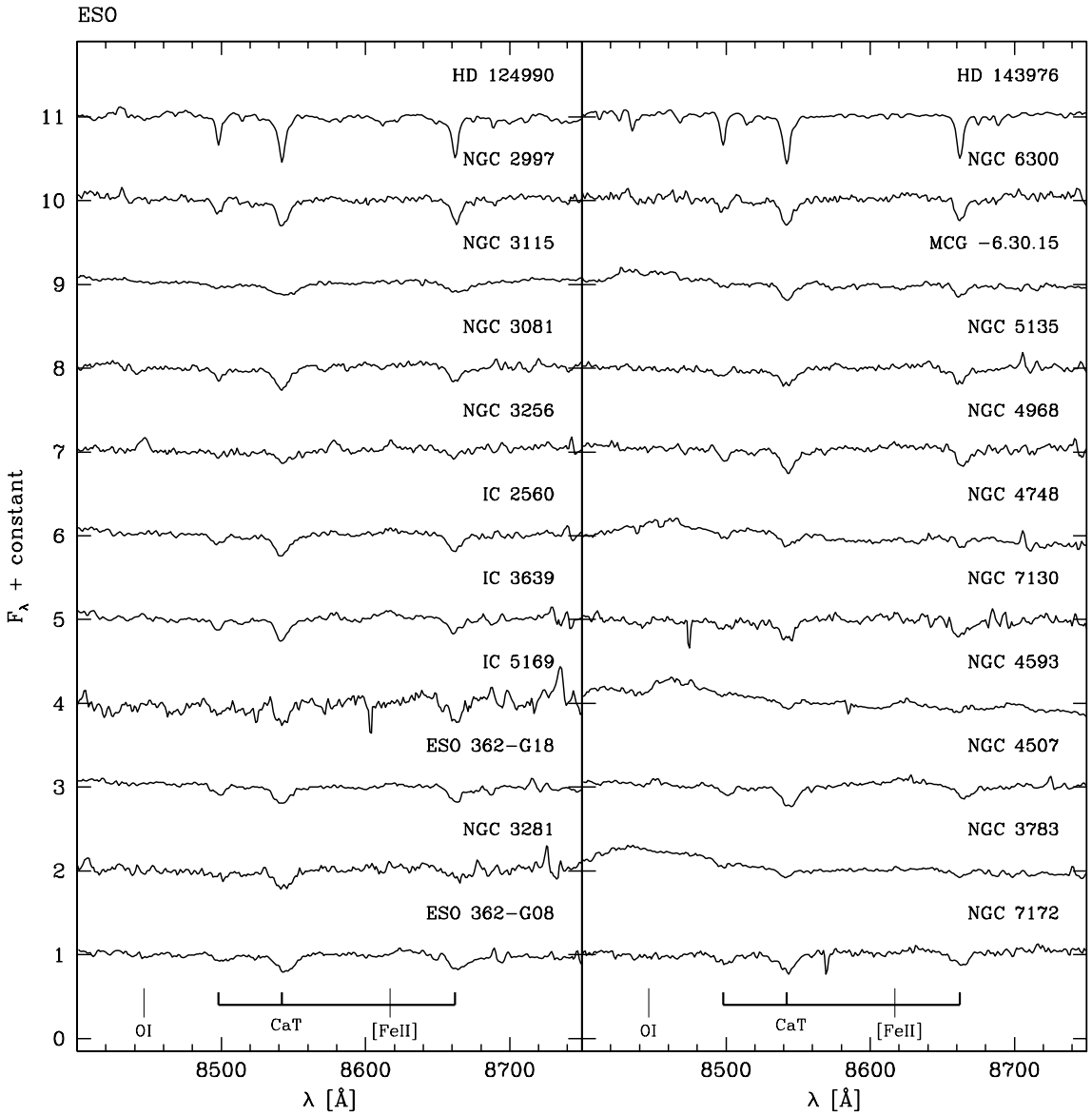

Figure 2. CaT spectra for the ESO 1.52-m observations. All spectra are normalized and shifted vertically for clarity. The top spectrum in each panel corresponds to a velocity standard star observed with the same instrumental set-up.

set-up, to illustrate the kinematical broadening in the galaxy spectra. The wavelengths of the CaT lines and other features are indicated. We recall that all spectra in this atlas correspond to the nuclear regions: 2 × 2.46 arcsec^2 for the ESO galaxies, 2 × 2.34 arcsec^2 for those observed at the KPNO 2.1-m and 1.5 × 2 arcsec^2 for those observed at the KPNO 4-m. Defining r_{ap} as the radius of a circle whose area equals the aperture area, our nuclear spectra correspond to physical regions of projected radii between $r_{ap} = 50$ and 700 pc of the nucleus, with a median value of 286 pc (Table 5).

All spectra were brought to the rest frame using, whenever possible, the mean redshift derived from the CaT absorption lines. For convenience, the spectra were normalized to the median flux in the

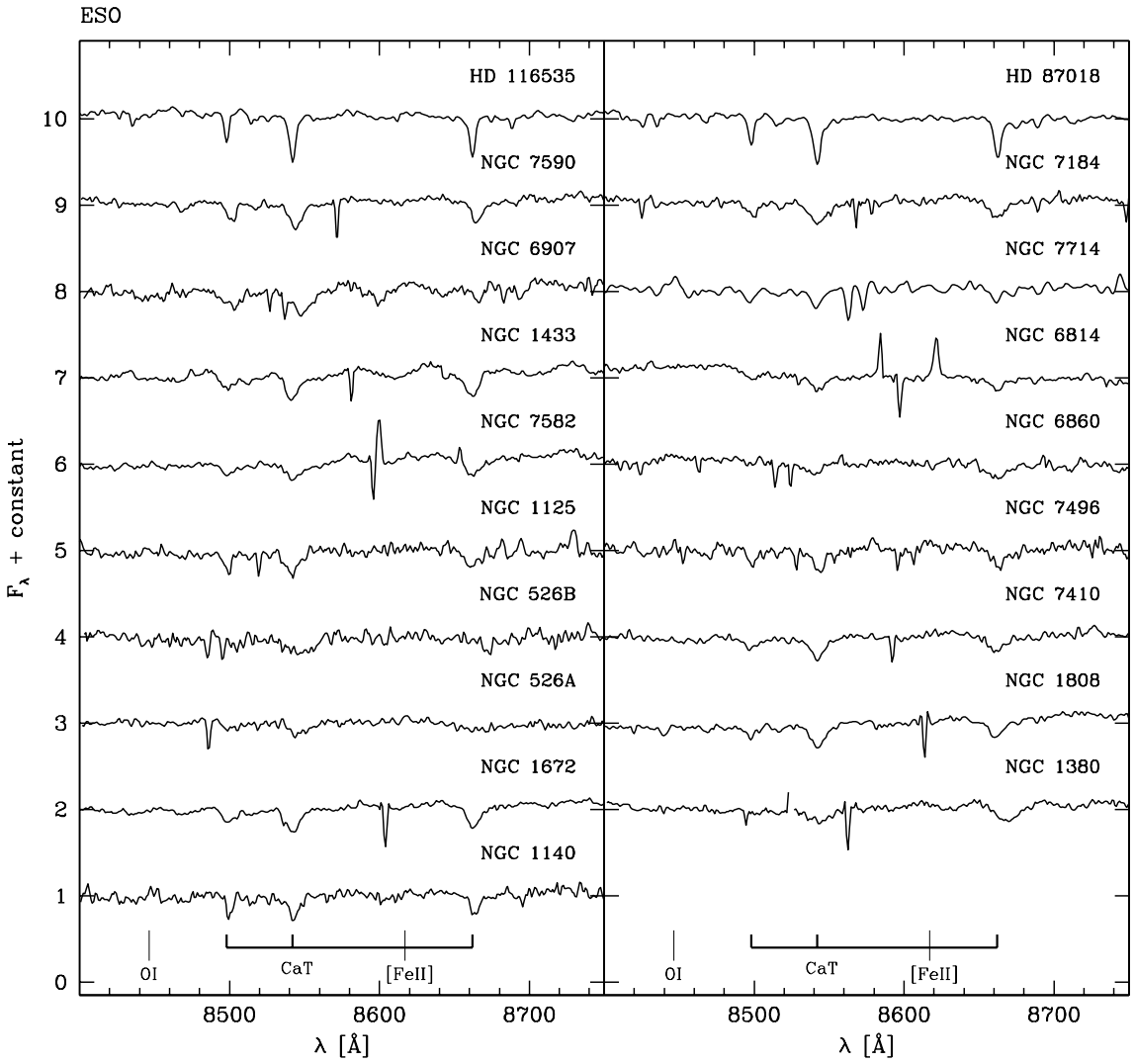

Figure 3. As Fig. 2.

8554–8574 Å interval. We estimate the signal-to-noise ratio (S/N) by the mean/rms flux ratio in this same window. The resulting S/N spans the 8–125 range, with a median S/N of 41.

Figs 2–6 show that our NIR spectra often contain features which complicate the analysis of the CaT, such as emission lines (narrow and broad), noise and imperfectly removed atmospheric features. To help to deal with this problem, we have assigned a 'quality flag' to each spectrum according to the degree of contamination of the CaT lines. Columns 8 of Tables 1–3 list the results. Quality 'a' refers to the best spectra, where the CaT lines are little or not affected by any of the problems above, as in NGC 2997, Mrk 573 and NGC 2639 (Figs 2, 4 and 5, respectively). Quality 'b' refers to reasonably good spectra, but where one of the CaT lines is contaminated. NGC 3281 (Fig. 2) and Mrk 3 (Fig. 4) are examples of quality 'b' spectra. Quality 'c' corresponds to problematic spectra, such as NGC 4748 and IRAS 01475−0740 in Figs 2 and 5, respectively. CaT measurements for these objects should be treated with caution. Finally, we define as quality 'd' those spectra that are so complex that it is impossible to derive any reasonably accurate CaT measurement. All such cases are presented in Fig. 6. Some Seyfert 1s and most narrow-line Seyfert 1s in our sample fall in this category. In this latter class, the CaT absorption lines are superposed to broad emission components of the same transitions from the broad-line region (Ferland & Persson 1989). AKN 564 and Mrk 1239 are two such cases. We have not attempted to disentangle the absorption and emission components in these cases. In some of these objects, useful CaT information can be obtained from off-nuclear extractions (Paper II).

The above classification allows us to investigate how our results are affected by data quality. As expected, the S/N tends to increase as one goes from quality 'c' to 'a'. The median values are S/N = 26, 37 and 47 for qualities 'c', 'b' and 'a', respectively. Also, the uncertainties in the CaT products (velocity dispersion and equivalent width) are smaller, the better the quality (Sections 4 and 5).

Our data comprise 40, 15 and 17 objects with quality flags 'a', 'b' and 'c', respectively, totaling 72 galaxies with useful CaT spectra. This statistically significant data set, which is similar in quality and quantity to that of NW, is analysed in the next sections.

3.2 [S III]λ9069 line

In 40 galaxies, the [S III]λ9069 line is detected with at least a reasonable quality line profile (equivalent width $\gtrsim$1 Å). The [S III] profiles are shown in Figs 7 and 8. We have fitted this line with a single Gaussian profile. The resulting values of its width, $\sigma_{[S\,III]}$ (corrected

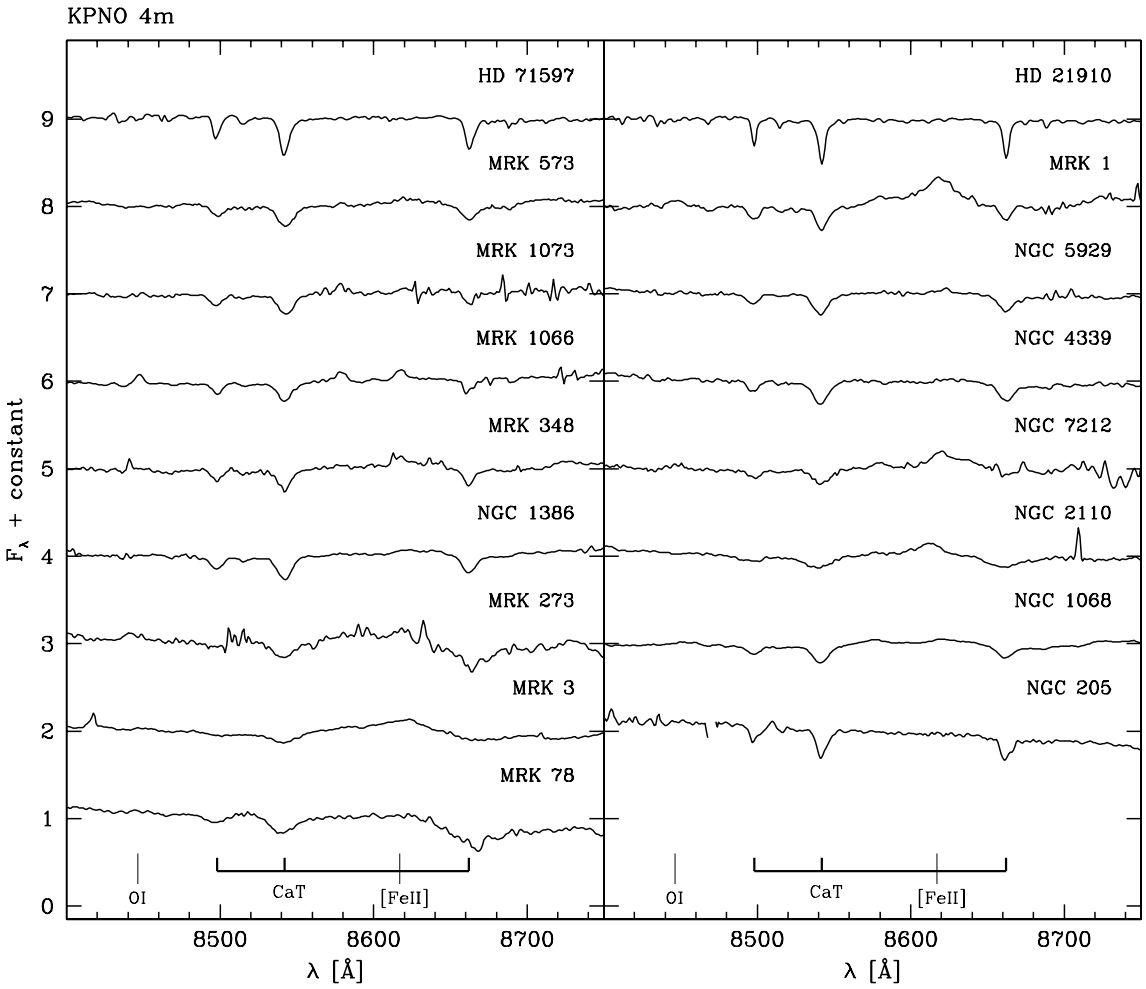

Figure 4. As Fig. 2, but for observations in the KPNO 4-m telescope.

for instrumental broadening) and equivalent width $W_{[\mathrm{S\,III}]}$ are listed in Table 6. We do not quote [S III] fluxes because of the uncertain absolute flux scale. The width of the [S III] line provides a rough measure of the typical velocity of clouds in the NLR of AGNs. In Paper II we compare this velocity with the typical stellar velocities deduced from the analysis of the CaT lines. In Paper II we also compare the $W_{[\mathrm{S\,III}]}$ values of type 1 and 2 Seyferts, which may indicate the diluting effects of an underlying AGN continuum at NIR wavelengths.

4 STELLAR VELOCITY DISPERSIONS

Because of its location in a relatively clean spectral region, the CaT is an ideal tracer of stellar kinematics in galaxies. This potential was recognized long ago in studies of normal galaxies (Pritchet 1978; Dressler 1984) and even AGNs (TDT). This is all the more true in AGNs, where optical kinematical tracers such as the Mg lines at ∼5175 Å are often contaminated by emission features, which complicates the measurement of kinematical properties (NW). The combination of this practical advantage with the discovery of the M_{BH}–$\sigma_\star$ relation brought renewed interest in the CaT as a tool to measure $\sigma_\star$, and thus indirectly weigh black holes, particularly in AGNs.

In this section we present measurements of $\sigma_\star$ for galaxies in our atlas. Two different methods were employed to estimate $\sigma_\star$. In what follows we describe these methods (Sections 4.1 and 4.2) and compare their results both with each other and with values in the literature (Section 4.3).

4.1 Direct fitting method

Kinematical parameters can be estimated by a direct fitting method (DFM), which consists of fitting a model to the observed CaT spectrum directly in λ-space (Barth et al. 2002). A model spectrum M_λ can be built combining one or more stellar templates with a continuum C_λ, and then convolving it with an assumed Gaussian line-of-sight velocity distribution function $G(v_\star, \sigma_\star)$, centred at $v_\star$ and broadened by $\sigma_\star$. The resulting expression for M_λ is

$$M_\lambda = M_{\lambda_0}\left(\sum_{j=1}^{N} x_j T_{j,\lambda} r_\lambda\right) \otimes G(v_\star, \sigma_\star). \quad (1)$$

(i) Here, $T_{\lambda,j}$ is the spectrum of the jth template star normalized at λ_0. The continuum C_λ is also included in the $T_{\lambda,j}$ base as a set of power laws with different slopes. Each galaxy was modelled with a base containing only velocity standard stars observed under the same instrumental set-up, thus circumventing the need for corrections due to different spectral resolutions.

(ii) $\boldsymbol{x}$ is a vector whose components x_j ($j = 1 \ldots N$) represent the fractional contribution of each base element to the total synthetic flux at λ_0, denoted by M_{λ_0}.

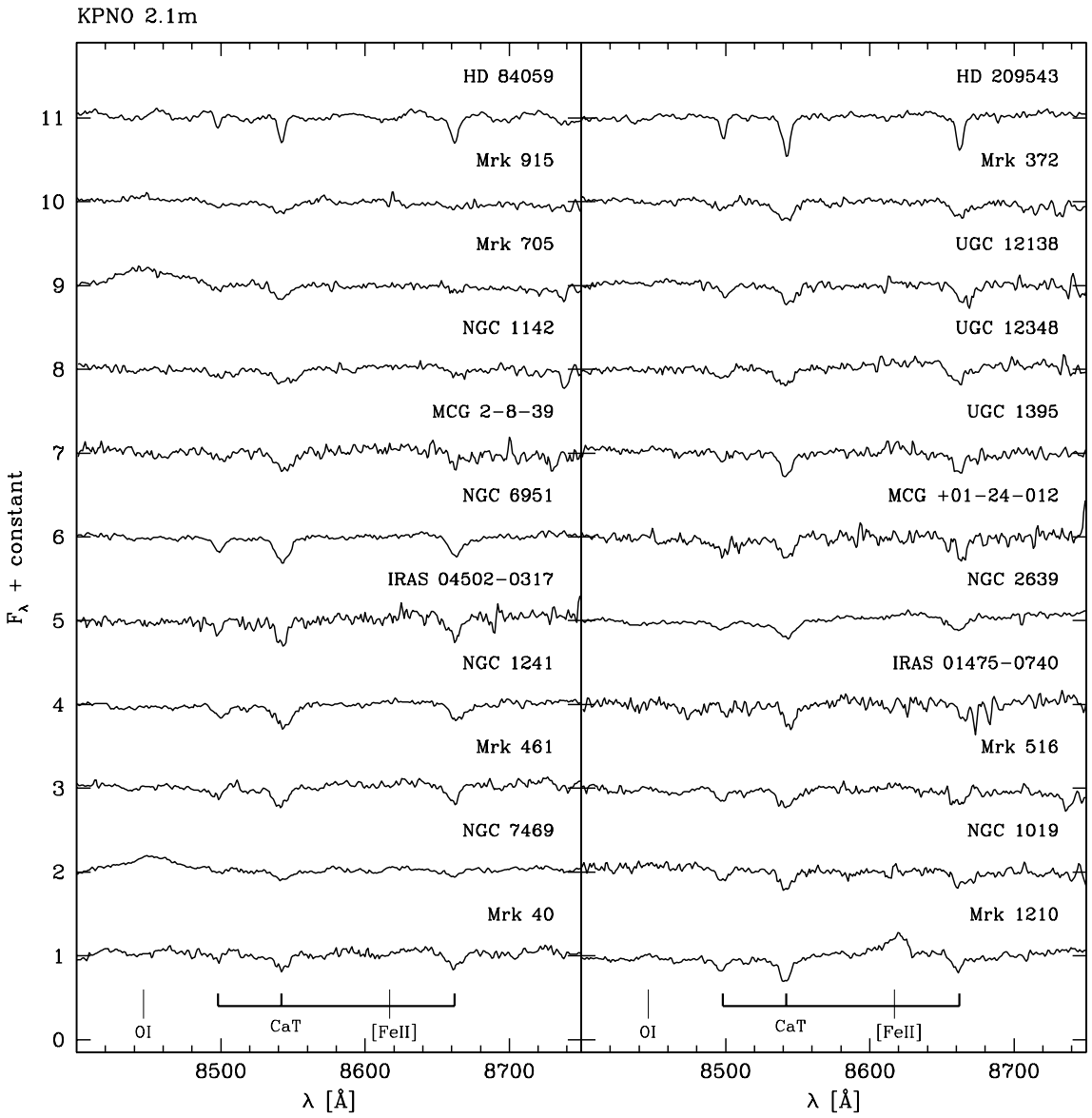

Figure 5. As Fig. 2, but for observations in the KPNO 2.1-m telescope.

(iii) $r_\lambda \equiv 10^{-0.4(A_\lambda - A_{\lambda_0})}$ accounts for reddening by a foreground dust screen.

The continuum components in the $T_{\lambda,j}$ base are introduced with the specific aim of allowing the fits to account for a possible mismatch between the velocity standard templates and the stars in the galaxy or dilution of the CaT by an underlying continuum. It is clear that we cannot hope to constrain well the shape of C_λ given the narrow spectral range of our data. Similarly, extinction is included in the fits just for completeness, because it cannot be well constrained by the data either. Indeed, of all $N_\star + 3$ parameters in the model we are only interested in one: $\sigma_\star$. The effect of $\sigma_\star$ upon M_λ is completely different from that of all the uninteresting parameters, which allows it to be well constrained by the data.

The fits are performed by minimizing the χ^2 between model and observed (O_λ) spectra

$$\chi^2 = \sum_\lambda [(O_\lambda - M_\lambda)\, w_\lambda]^2 \qquad (2)$$

where the weight spectrum w_λ is defined as the inverse of the noise in O_λ. Emission lines and spurious features, such as residual sky lines, are masked out by setting $w_\lambda = 0$. Except for the spectral base and wavelength range, this method is identical to that in Cid Fernandes et al. (2004, 2005), who fit the optical spectra of galaxies by a combination of evolutionary synthesis models with the code STARLIGHT. In fact, exactly the same code was used in our fits. We thus refer the reader to those papers for details on the numerical aspects of the fits.

Fig. 9 illustrates some of the resulting fits. In objects with clean CaT spectra (e.g. NGC 1241 and 2997), spectral regions outside the CaT lines were included in the fit, but we emphasize that ignoring them yields practically identical values of $\sigma_\star$. For more problematic spectra (e.g. Mrk 3 and Mrk 705), we have chosen to concentrate the fits on the CaT lines, masking out other wavelengths. The exact choice of the mask affects the derived values of $\sigma_\star$, but these variations are well within the uncertainties $\Delta\sigma_\star$ estimated below. Table 6 lists the resulting values of $\sigma_\star$.

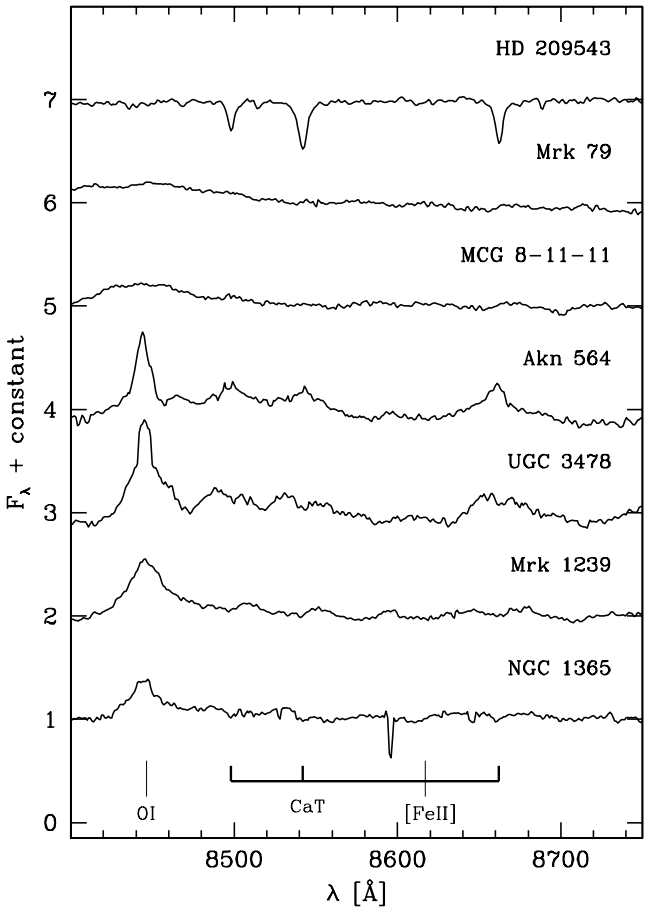

Figure 6. Objects containing complex (quality flag 'd') spectra in the CaT region.

The uncertainty in $\sigma_\star$ was estimated by the method outlined in Barth et al. (2002), which basically consists of finding the range in $\sigma_\star$ that causes an increase of $\Delta\chi^2 = 1$ over the best fit, after rescaling the errors to yield a best-fitting reduced χ^2 of 1. We find $\Delta\sigma_\star$ in the 3–24 km s^{-1} range (Table 6). Separating spectra according to their quality flags, we find median values of $\Delta\sigma_\star = 6$, 10 and 12 km s^{-1} for quality 'a', 'b' and 'c', respectively.

An independent assessment of the uncertainties is possible in the cases of Mrk 1210 and NGC 7130, for which we have repeated observations with different telescopes. For Mrk 1210, we obtain $\sigma_\star = 72 \pm 9$ and 77 ± 7 km s^{-1} for the ESO and KPNO 2.1-m observations, respectively, while for NGC 7130 we derive $\sigma_\star = 140 \pm 8$ and 112 ± 9 km s^{-1} for the ESO and KPNO 4-m data. In both cases the independent measurements are consistent to within $\sim 2\sigma$ confidence.

A more traditional method to estimate $\Delta\sigma_\star$ consists of evaluating the dispersion among fits performed using individual template stars (e.g. Tonry & Davis 1979). For completeness, we have also evaluated $\Delta\sigma_\star$ with this method. The uncertainties obtained in this way are $\sim$30 per cent larger than those obtained by the method described above. This agreement is hardly surprising, given that template mismatch is already accounted for in our implementation of the DFM, which includes a library of template stars in the base $T_{j,\lambda}$ (equation 1). When performing fits with a fixed $\sigma_\star$, as we do in the estimation of $\Delta\sigma_\star$ following the methodology of Barth et al. (2002), the fractions x_j associated with each template star are allowed to vary freely, which is qualitatively equivalent to changing the template star. Hence, unlike in Barth et al. (2002), there is no need to add these two estimates of $\Delta\sigma_\star$ in quadrature to obtain a total error estimate. (Doing that would increase $\Delta\sigma_\star$ by $\sim$60 per cent with respect to the values listed in Table 6.)

4.2 Cross-correlation method

One of the first techniques devised to measure velocity dispersions in galaxies was the cross-correlation method (CCM; Tonry & Davis 1979). NW review this method and show that in the CaT region it yields fairly good results. In this work, the IRAF task FXCOR was used. In few words, FXCOR finds the cross-correlation function between the galaxy and the template spectra in Fourier space. The peak of this function is then modelled by a Gaussian. We use the same individual masks which were used in the DFM, and we allow a linear continuum subtraction from the galaxy spectra. The output from FXCOR is calibrated in order to account for instrumental resolution. Column 3 of Table 6 presents $\sigma_\star$ values obtained with this method. Uncertainties in this case are evaluated from the rms in $\sigma_\star$ values obtained using different template stars.

We find that the DFM and the CCM yield velocity dispersions consistent to within 19 km s^{-1} on average. The agreement is much better for quality 'a' spectra, for which the difference between $\sigma_\star^{\rm DFM}$ and $\sigma_\star^{\rm CCM}$ is just 9 km s^{-1} in the rms. For quality 'b' and 'c' the DFM and CCM methods agree to rms dispersions of 20 and 30 km s^{-1}, respectively, which further confirms that data quality is the major source of uncertainty in $\sigma_\star$. The uncertainties $\Delta\sigma_\star$ obtained with these two methods are also similar, with an rms difference of 6 km s^{-1}.

4.3 Comparison with previous results

In Fig. 10 we compare our DFM measurements of $\sigma_\star$ with values compiled from the literature for objects in common. The two major sources of $\sigma_\star$ are NW and Cid Fernandes et al. (2004), which have 14 and 22 objects in common with our sample, respectively. NW derive $\sigma_\star$ from the CCM applied to either the CaT or the Mg lines in the optical, while Cid Fernandes et al. (2004) estimate $\sigma_\star$ fitting the 3500–5200 Å spectra of Seyfert 2s with a combination of single stellar populations from the Bruzual & Charlot (2003, hereafter BC03) models. These two studies agree in their estimates of $\sigma_\star$ at the level of $\pm$21 km s^{-1} rms.

Our CaT-based estimates of $\sigma_\star$ are in good agreement with these previous estimates. The rms difference between our values and those in the literature is 22 km s^{-1}. The spread is somewhat smaller for quality 'a' data (rms of 21 km s^{-1}) than for qualities 'b' and 'c' (25 km s^{-1}). Furthermore, on average, our estimates of $\sigma_\star$ are just 4 km s^{-1} lower than those in the literature. Very similar results are obtained comparing our CCM-based estimates of $\sigma_\star$ with literature data, which also yield an rms of 22 km s^{-1}. Given the differences in data quality, spatial extractions, method of analysis, and the intrinsic uncertainties in $\sigma_\star$, we conclude that there are no significant differences between our estimates of $\sigma_\star$ and those reported in previous studies. In any case, the level of agreement is very similar to those among other studies.

We also made a compilation from Oliva et al. (1995, 1999) NIR CO and Si $\sigma_\star$ estimates, where we can find nine objects in common with our sample. Although the two estimates are very likely to be correlated ($P_{\rm rs} \approx 2.5$ per cent), here the difference between results is higher than when compared with optical data, indicating that our estimated $\sigma_\star$ is, on average, lower by 34 km s^{-1}. Considering just the six objects that have an 'a' fitting quality, this difference practically

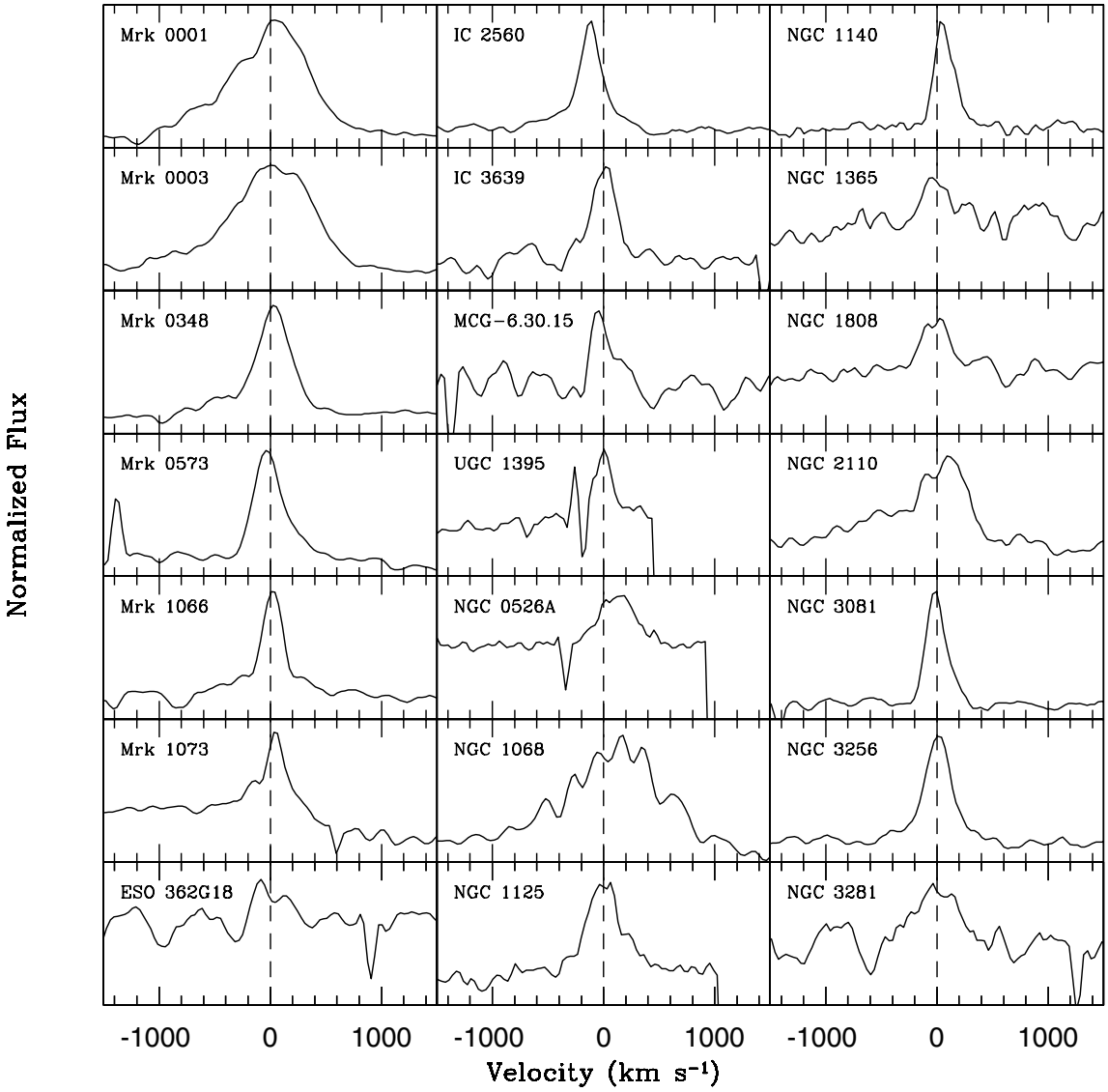

Figure 7. [S III]λ9069 emission-line profiles, normalized to the continuum level.

does not change (33 km s^{-1}), having an rms of 38 km s^{-1} (i.e. it agrees with our results within a 2σ confidence level, considering that their errors are also of 20 km s^{-1}).

5 EQUIVALENT WIDTHS

Besides its use as a tracer of stellar kinematics, the CaT provides information on the properties of stellar populations in galaxies. The most extensive and up-to-date studies of the CaT in stars and as a diagnostic of stellar populations in galaxies have been published by Cenarro and co-workers in the last few years (Cenarro et al. 2001a,b, 2002, 2003; Vazdekis et al. 2003). As summarized in the introduction (see also Paper II), recent work reveals serious difficulties in interpreting the observed strength of the CaT in normal galaxies, which in turn raises doubts as to the usefulness of the CaT as a stellar population diagnostic. Clearly, the situation in AGNs ought to be even more problematic than for normal galaxies, given (i) the presence of emission lines around the CaT, (ii) the fact that many AGNs are known to be surrounded by starbursts of various ages and intensities, and (iii) the presence of an underlying non-stellar continuum, seen either directly (in Seyfert 1s) or scattered (Seyfert 2s).

Notwithstanding these caveats, in this section we present measurements of the CaT equivalent width for objects in our sample. These data are used in Paper II to evaluate the presence of an AGN continuum at NIR wavelengths, and to investigate how our AGNs fit into the CaT–$\sigma_\star$ relation (e.g. Michielsen et al. 2003).

We measure the CaT strength following Cenarro et al. (2001a), who offer two definitions of the CaT equivalent width: 'CaT' (which we call $W_{\rm CaT}$), which consists of a sum of the equivalent widths of all three CaT lines, and 'CaT*' (called $W_{\rm CaT*}$ here), which corrects $W_{\rm CaT}$ for contamination by Paschen line absorption. These equivalent widths are measured with respect to a continuum defined by fitting the spectrum in five windows in the 8474–8792 Å range.

It is evident from Figs 2–5 that this recipe cannot be blindly applied to our spectra, given the presence of emission lines, atmospheric and noise artefacts which affect both the continuum, CaT and Paschen bandpasses. On the other hand, in Section 4.1 we have seen that the DFM provides good matches to the clean regions of the spectra. Naturally, these model spectra do not suffer from the

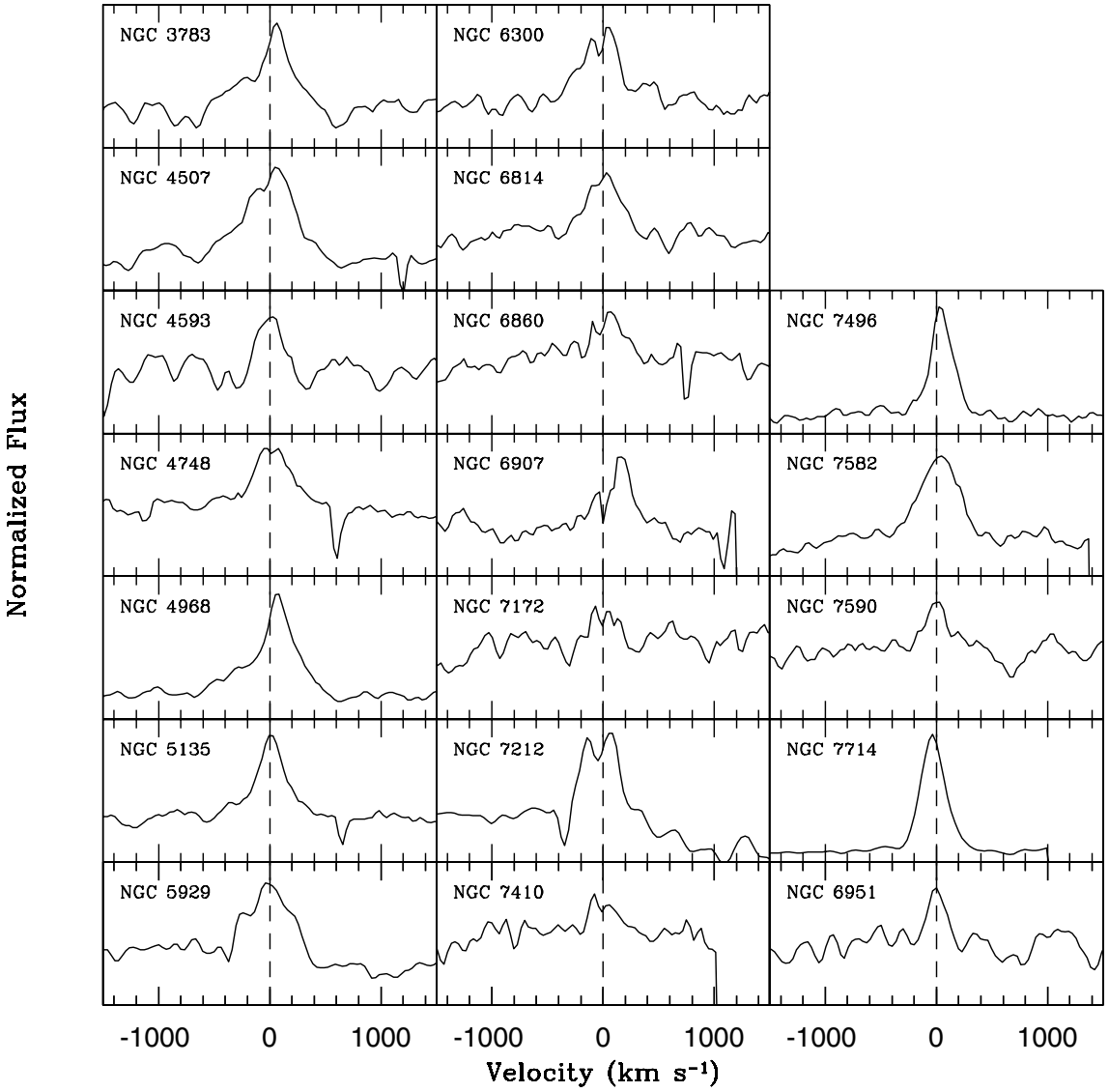

Figure 8. As Fig. 7.

aforementioned problems. Measuring the CaT indices over the model fits is therefore a simpler alternative to removing the unwanted features from the observed spectra. (A similar strategy was employed by Cid Fernandes et al. 2004 in their analysis of optical spectra of Seyfert 2s.) We thus opted to measure both $W_{\rm CaT}$ and $W_{\rm CaT*}$ over the synthetic spectra.

We tested the validity of this procedure by comparing the values of $W_{\rm CaT}$ measured for the model (M_λ) and observed (O_λ) spectra for galaxies with no serious contamination, or galaxies where the spurious features can be easily removed (say, by chopping narrow emission lines). We find that these two estimates of $W_{\rm CaT}$ agree well, with an rms difference of 0.4 Å. There is a small bias, in the sense that $W_{\rm CaT}$ values measured over the synthetic spectra are on average 0.5 Å smaller than those measured over the observed spectrum, generally due to noise in the redder continuum band. Both this offset and the rms difference are comparable to the formal uncertainties in $W_{\rm CaT}$. We thus conclude that this experiment validates our strategy of measuring $W_{\rm CaT}$ over the model spectra.

Although Cenarro et al. (2001a) and subsequent studies of normal galaxies favour $W_{\rm CaT*}$ over $W_{\rm CaT}$ as a measure of the CaT strength, we have reasons for the opposite choice. First, in several cases our DFM fits concentrate on windows centred nearly exclusively on the CaT lines. Hence, Paschen lines, even if present in the spectrum (which is not the case in any of our spectra, with the possible exception of the normal galaxy NGC 6907), would not have a relevant weight in the spectral fits. Secondly, only the KPNO 2.1-m observations include velocity standard stars with Paschen absorption lines in their spectra (F giants; see Table 4). For the other runs, the spectral base $T_{j,\lambda}$ does not cover such spectral types, so the synthetic spectrum cannot possibly model any Paschen line absorption properly, thus rendering the Paschen line correction in $W_{\rm CaT*}$ meaningless. Hence, we only present $W_{\rm CaT}$ measurements (Table 6).

Because the M_λ spectra are effectively noiseless, in order to compute uncertainties in $W_{\rm CaT}$ we carried out a formal propagation using the S/N derived for each galaxy (Section 3.1). To be on the conservative side, we further add 0.5 Å in quadrature to account for the empirically established rms difference between $W_{\rm CaT}$ measurements performed over M_λ and over clean O_λ spectra. The median uncertainties are $\Delta W_{\rm CaT} = 0.6$, 0.7 and 0.8 Å for quality 'a', 'b' and 'c' spectra respectively.

Inspection of the $W_{\rm CaT}$ values in Table 6 shows that this index spans a range of values from ∼1 to 9 Å. However, most values

Table 6. Columns 2 and 3 give the velocity dispersions obtained with the DFM and CCM methods, respectively. Columns 4 and 5 give the width and equivalent width of the [S III]λ9069 emission line. Uncertain measurements are marked with ':'. Column 6 gives the CaT equivalent width.

Object	$\sigma_\star^{\rm DFM}$ (km s^{-1})	$\sigma_\star^{\rm CCM}$ (km s^{-1})	$\sigma_{\rm [S\,III]}$ (km s^{-1})	$W_{\rm [S\,III]}$ (Å)	$W_{\rm CaT}$ (Å)
ESO 362-G08	179 ± 7	193 ± 10			7.2 ± 0.3
ESO 362-G18	126 ± 5	134 ± 4	132:	3:	6.7 ± 0.3
IC 2560	135 ± 4	138 ± 5	107	16	7.8 ± 0.4
IC 3639	95 ± 5	99 ± 5	111	10	6.3 ± 0.3
IC 5169	114 ± 12	111 ± 2			7.5 ± 0.9
IRAS 01475−0740	62 ± 11	108 ± 17			6.0 ± 0.3
IRAS 04502−0317	74 ± 8	74 ± 15			6.8 ± 0.5
MCG +01-24-012	84 ± 10	92 ± 18			6.8 ± 0.7
MCG −6.30.15	94 ± 8	103 ± 4	90	5	5.1 ± 0.5
MCG 2-8-39	170 ± 13	126 ± 11			8.0 ± 0.8
MRK 1	86 ± 4	79 ± 4	375	86	6.2 ± 0.5
MRK 3	228 ± 13	249 ± 4	364	42	4.2 ± 0.4
MRK 78	201 ± 8	186 ± 4			7.3 ± 0.3
MRK 273	211 ± 14	186 ± 2			7.7 ± 0.7
MRK 348	95 ± 6	98 ± 8	179	40	6.3 ± 0.2
MRK 573	147 ± 5	148 ± 3	171	28	7.9 ± 0.1
MRK 1066	100 ± 4	90 ± 6	119	21	5.9 ± 0.4
MRK 1073	114 ± 6	109 ± 5	168	24	5.9 ± 0.5
Mrk 40	125 ± 7	116 ± 4			4.0 ± 0.4
Mrk 372	155 ± 6	161 ± 5			6.4 ± 0.5
Mrk 461	111 ± 6	123 ± 4			5.6 ± 0.4
Mrk 516	113 ± 12	114 ± 7			7.4 ± 0.6
Mrk 705	128 ± 11	120 ± 15			5.1 ± 0.3
Mrk 915	181 ± 18	146 ± 16			5.2 ± 0.6
Mrk 1210	77 ± 7	82 ± 16			6.7 ± 0.4
NGC 205	47 ± 6	74 ± 6			6.2 ± 0.2
NGC 526A	198 ± 16	219 ± 11	159	4	4.7 ± 0.5
NGC 526B	237 ± 22	167 ± 11			7.0 ± 1.1
NGC 1019	106 ± 9	110 ± 11			6.5 ± 0.5
NGC 1068	140 ± 6	147 ± 3	543	120	6.3 ± 0.4
NGC 1125	118 ± 9	138 ± 6	168	11	7.6 ± 0.5
NGC 1140	53 ± 6	60 ± 3	81	12	5.9 ± 0.7
NGC 1142	219 ± 15	202 ± 47			8.6 ± 0.4
NGC 1241	136 ± 5	142 ± 12			8.5 ± 0.4
NGC 1380	250 ± 16	215 ± 8			7.8 ± 2.4
NGC 1386	123 ± 3	133 ± 3			8.1 ± 0.2
NGC 1433	98 ± 6	113 ± 3			7.6 ± 0.4
NGC 1672	108 ± 4	111 ± 3			7.7 ± 0.2
NGC 1808	119 ± 6	129 ± 4	129	2	7.3 ± 0.4
NGC 2110	264 ± 11	273 ± 7	375	16	6.4 ± 0.3
NGC 2639	168 ± 6	155 ± 12			7.2 ± 0.2
NGC 2997	79 ± 4	89 ± 4			8.0 ± 0.4
NGC 3081	129 ± 8	113 ± 4	77	20	7.4 ± 0.4
NGC 3115	275 ± 6	268 ± 8			7.0 ± 0.4
NGC 3256	130 ± 13	100 ± 6	120	17	3.7 ± 0.5
NGC 3281	161 ± 8	176 ± 3	235	8	7.3 ± 0.4
NGC 3783	116 ± 20	114 ± 6	247	17	3.0 ± 0.2
NGC 4339	123 ± 3	129 ± 3			7.4 ± 0.2
NGC 4507	146 ± 7	152 ± 4	229	16	7.0 ± 0.4
NGC 4593	153 ± 24	105 ± 5	96	3	3.4 ± 0.3
NGC 4748	76 ± 15	78 ± 13	187	10	3.4 ± 0.5
NGC 4968	105 ± 9	106 ± 4	182	16	6.9 ± 0.5
NGC 5135	128 ± 8	124 ± 6	135	10	6.1 ± 0.4
NGC 5929	119 ± 4	122 ± 4	195	9	6.5 ± 0.2
NGC 6300	92 ± 5	110 ± 5	217	7	8.3 ± 0.4
NGC 6814	83 ± 11	113 ± 6	169	5	4.0 ± 0.3
NGC 6860	162 ± 11	141 ± 5	153:	3:	5.6 ± 0.6
NGC 6907	157 ± 12	195 ± 15	199	6	9.2 ± 1.0
NGC 6951	115 ± 4	113 ± 12	73	2	9.0 ± 0.3

Table 6 – *continued*

Object	$\sigma_\star^{\rm DFM}$ (km s^{-1})	$\sigma_\star^{\rm CCM}$ (km s^{-1})	$\sigma_{\rm [S\,III]}$ (km s^{-1})	$W_{\rm [S\,III]}$ (Å)	$W_{\rm CaT}$ (Å)
NGC 7130	141 ± 8	147 ± 5			6.9 ± 0.4
NGC 7172	154 ± 6	160 ± 9	112:	1:	6.9 ± 1.1
NGC 7184	146 ± 7	131 ± 5			7.9 ± 1.2
NGC 7212	143 ± 10	140 ± 2	164	26	5.3 ± 0.2
NGC 7410	144 ± 7	144 ± 6	126:	1:	7.7 ± 0.4
NGC 7469	125 ± 12	144 ± 11			2.9 ± 0.2
NGC 7496	76 ± 10	94 ± 6	96	15	5.8 ± 0.7
NGC 7582	121 ± 7	113 ± 3	180	8	5.9 ± 0.5
NGC 7590	93 ± 4	90 ± 4	136	2	7.7 ± 2.0
NGC 7714	59 ± 9	65 ± 4	105	28	4.7 ± 2.4
UGC 1395	66 ± 6	62 ± 16	47:	4:	6.5 ± 0.4
UGC 12138	115 ± 10	136 ± 8			6.9 ± 0.6
UGC 12348	155 ± 9	165 ± 14			7.6 ± 0.4

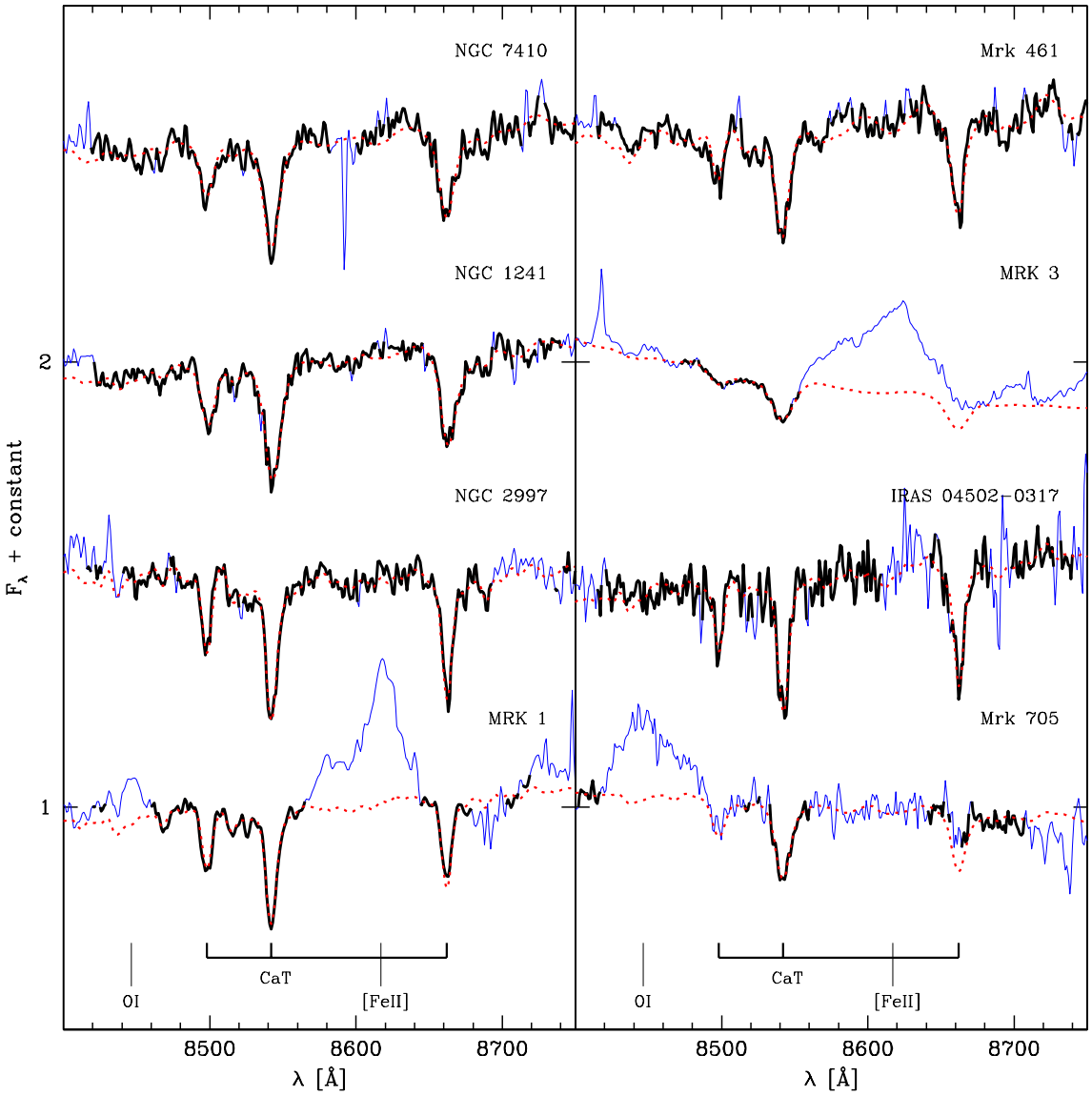

Figure 9. Examples of fits to the galaxy spectra. The solid line shows the observed spectrum, while the dotted line shows the spectral fits obtained with the DFM. A thicker line is used to mark the region actually used in the fits. NGC 7410, 1241, 2997 and Mrk 1 have quality flag 'a', Mrk 461 and Mrk 3 have quality 'b', and IRAS 04502−0317 and Mrk 705 have quality 'c'.

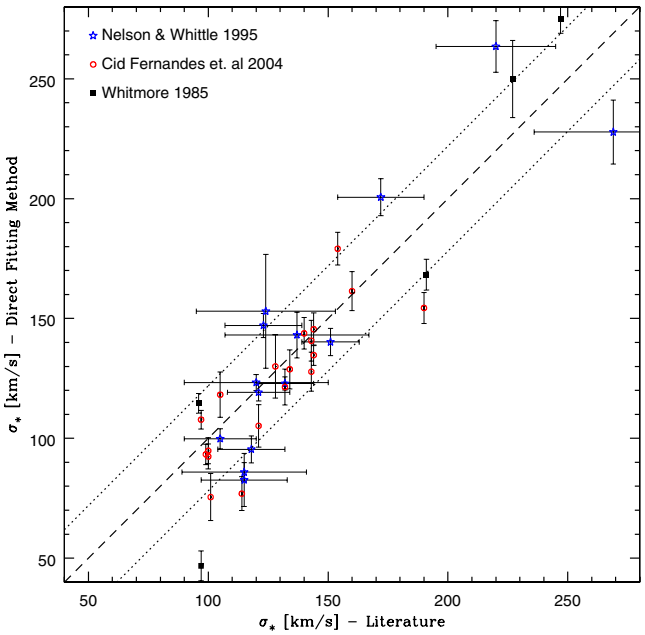

Figure 10. Comparison of the stellar velocity dispersions estimated in this work and values compiled from the literature. The identity line is traced by the dashed line, while dotted lines indicate the ± 22 km s^{-1} global dispersion ($=1\sigma$).

are within the 6–8 Å range, giving the false impression that stellar populations are very homogeneous in our sample. This is definitely not true, as we know from independent work at other wavelengths for many of the same galaxies studied here (e.g. Cid Fernandes et al. 2001, 2004). Instead, the small variation in CaT strength reinforces the notion that this feature is not much sensitive to stellar population properties. The only noticeable trend is that Seyfert 1s tend to have weaker CaT than other galaxies. On the mean, $W_{\rm CaT} = 4.6 \pm 2.0$ Å (sample dispersion) for Seyfert 1s and 7.0 ± 1.0 Å for Seyfert 2s. The statistics for the three starbursts in our sample is 4.7 ± 1.1 Å, while for the remaining six non-active galaxies $W_{\rm CaT} = 7.7 \pm 1.0$ Å, very similar to the values spanned by Seyfert 2s. The most likely origin for the difference between type 1 and type 2 AGNs is dilution by an underlying non-stellar FC in type 1s. Hence, if on the one hand $W_{\rm CaT}$ turns out to be a rather poor tracer of stellar populations, it seems to be a good FC detector. These aspects are explored in greater depth in Paper II.

6 CONCLUSIONS

In this paper we have presented a spectroscopic atlas of 78 galaxies in the region around the CaT. Most of the objects are AGNs, split into 43 type 2 Seyferts and 26 type 1s. The spectra cover the inner $r_{\rm pc} \sim 300$ pc with a typical S/N of 40. Quality flags were assigned to each spectrum to describe the degree of contamination of the CaT absorption lines by emission lines or atmospheric features. The main products from our analysis of this data set are stellar velocity dispersions, [S III]λ9069 line profiles and CaT equivalent widths.

Stellar velocity dispersions ($\sigma_\star$) were measured for 72 of the spectra using both direct fitting and CCMs. The two techniques yield results compatible to within an rms of 19 km s^{-1}, which is also the typical uncertainty of our estimates. Comparison with $\sigma_\star$ values reported in the literature for objects in common agree with our estimates at the level of $\sim$20 km s^{-1} rms for optical data, and at a 2σ level for NIR data.

We have also analysed the [S III]λ9069 line profiles for 40 galaxies in the sample with useful data in this range. Single Gaussian fits were performed, producing estimates of line width and equivalent width.

The CaT equivalent width was measured over the synthetic spectra obtained from the direct fits, circumventing the manual editing of the spectra that would be required to remove undesirable features which affect $W_{\rm CaT}$. We find that the value of $W_{\rm CaT}$ in Seyfert 2s and normal galaxies are concentrated in a relatively small range, from $\sim$6 to 8 Å. Type 1 Seyferts tend to have a weaker CaT, most likely due to dilution by a non-stellar continuum.

These data products are analysed in Paper II, where we investigate the relation between nebular and stellar kinematics and the behaviour of the CaT strength as a function of activity type and stellar population properties.

ACKNOWLEDGMENTS

AGR, LRV, NVA, RCF and TSB acknowledge the support from CAPES, CNPq and Instituto do Milênio. RGD acknowledges support by Spanish Ministry of Science and Technology (MCYT) through grant AYA-2004-02703. AGR and LRV acknowledge A. Rodríguez-Ardila for suggestions in the reduction process. We thank the Laboratório Nacional de Astrofísica for the allocation of time on the ESO 1.52-m and financial support during the runs. Some of the data described here were taken at the KPNO, National Optical Astronomy Observatories, which are operated by AURA, Inc., under a cooperative agreement with the National Science Foundation. Basic research at the US Naval Research Laboratory is supported by the Office of Naval Research. This research made use of the NED, which is operated by the Jet Propulsion Laboratory, Caltech, under contract with NASA.

REFERENCES

Barth A. J., Ho L. C., Sargent W. L. W., 2002, ApJ, 566, L13
Barth A. J., Ho L. C., Sargent W. L. W., 2003, ApJ, 583, 134
Barth A. J., Ho L. C., Rutledge R. E., Sargent W. L. W., 2004, ApJ, 607, 90
Barth A. J., Greene J. E., Ho L. C., 2005, ApJ, 619, L151
Bassani L., Dadina M., Maiolino R., Salvati M., Risaliti G., Della Ceca R., Matt G., Zamorani G., 1999, ApJS, 121, 473
Botte V., Ciroi S., di Mille F., Rafanelli P., Romano A., 2004, MNRAS, 356, 789
Bruzual G., Charlot S., 2003, MNRAS, 344, 1000 (BC03)
Cardelli J. A., Clayton G. C., Mathis J. S., 1989, ApJ, 345, 245
Cenarro A. J., Cardiel N., Gorgas J., Peletier R. F., Vazdekis A., Prada F., 2001a, MNRAS, 326, 959
Cenarro A. J., Gorgas J., Cardiel N., Pedraz S., Peletier R. F., Vazdekis A., 2001b, MNRAS, 326, 981
Cenarro A. J., Gorgas J., Cardiel N., Vazdekis A., Peletier R. F., 2002, MNRAS, 329, 863
Cenarro A. J., Gorgas J., Vazdekis A., Cardiel N., Peletier R. F., 2003, MNRAS, 339, 12
Cenarro A. J., Sánchez-Blázquez P., Cardiel N., Gorgas J., 2004, ApJ, 614, 101
Cid Fernandes R., Terlevich R. J., 1995, MNRAS, 272, 423
Cid Fernandes R., Heckman T., Schmitt H., González Delgado R. M., Storchi-Bergmann T., 2001, ApJ, 558, 81
Cid Fernandes R., Gu Q., Melnick J., Terlevich E., Terlevich R., Kunth D., Rodrigues Lacerda R., Joguet B., 2004, MNRAS, 355, 273
Cid Fernandes R., Mateus A., Sodré L., Stasinska G., Gomes J. M., 2005, MNRAS, 358, 363

de Vaucouleurs G., de Vaucouleurs A., Corwin H. G. Jr., Buta R. J., Paturel G., Fouque P., 1991, Third Reference Catalogue of Bright Galaxies, Vols 1–3. Springer-Verlag, Berlin
Dressler A., 1984, ApJ, 286, 97
Falcón-Barroso J., Peletier R. F., Vazdekis A., Balcells M., 2003, ApJ, 588, 17
Ferland G. J., Persson S. E., 1989, ApJ, 347, 656
Ferrarese L., Merritt D., 2000, ApJ, 539, 9
Ferrarese L., Pogge R. W., Peterson B. M., Merritt D., 2001, ApJ, 555, L79
Filippenko A. V., Ho L. C., 2003, ApJ, 588, L13
Gebhardt K. et al., 2000, ApJ, 539, 13
González Delgado R., Heckman T., Leitherer C., 2001, ApJ, 546, 845
Hamuy M., Suntzeff N. B., Heathcote S. R., Walker A. R., Gigoux P., Phillips M. M., 1994, PASP, 106, 566
Heckman T. et al., 1995, ApJ, 452, 549
Heckman T., González Delgado R., Leitherer C., Meurer G., Krolik J., Wilson A. S., Koratkar A., Kinney A., 1997, ApJ, 482, 114
Horne K., 1986, PASP, 98, 609
Jiménez-Benito L., Díaz A. I., Terlevich R. J., Terlevich E., 2000, MNRAS, 317, 907
Massey P., Gronwall C., 1990, ApJ, 358, 344
Massey P., Strobel K., Barnes J. V., Anderson E., 1988, ApJ, 328, 315
Michielsen D., De Rijcke S., Dejonghe H., Zeilinger W. W., Hau G.K. T., 2003, ApJ, 597, 21
Nelson C. H., Whittle M., 1995, ApJS, 99, 67
Nelson C. H., Whittle M., 1996, ApJ, 465, 96
Nelson C. H., Green R. F., Bower G., Gebhardt K., Weistrop D., 2004, ApJ, 615, 652
Oke J. B., 1990, AJ, 99, 1621
Oliva E., Origlia L., Kotilainen J. K., Moorwood A. F. M., 1995, A&A, 301, 55
Oliva E., Origlia L., Maiolino R., Moorwood A. F. M., 1999, A&A, 350, 90
Onken C. A., Ferrarese L., Merritt D., Peterson B. M., Pogge R. W., Vestergaard M., Wandel A., 2004, ApJ, 615, 645
Plait P., Bohlin R., 1997, Fringe science: creating a STIS CCD fringe flat field, in Casertano S., Jedrzejewski R., Keyes C. D., Stevens M., eds, The 1997 HST Calibration Workshop. Space Telescope Science Institute, Baltimore, MD
Pritchet C., 1978, ApJ, 221, 507
Saglia R. P., Maraston C., Thomas D., Bender R., Colless M., 2002, ApJ, 579, 13
Schlegel D., Finkbeiner D., Davis M., 1998, ApJ, 500, 525
Schmitt H., Donley J. L., Antonucci R. R. J., Hutchings J. B., Kinney A. L., 2003, ApJS, 148, 327
Storchi-Bergmann T., Kinney A. L., Challis P., 1995, ApJS, 98, 103
Terlevich E., Díaz A. I., Terlevich R. J., 1990, MNRAS, 242, 271 (TDT)
Thomas D., Maraston C., Bender R., 2003, MNRAS, 343, 279
Tonry J., Davis M., 1979, AJ, 84, 1511
Tremaine S. et al., 2002, ApJ, 574, 740
Vazdekis A., Cenarro A. J., Gorgas J., Cardiel N., Peletier R. F., 2003, MNRAS, 340, 1317
Whitmore B. C., McElroy D. B., Tonry J. L., 1985, ApJS, 59, 1
Whittle M., 1992, ApJS, 79, 49

This paper has been typeset from a TEX/LATEX file prepared by the author.